BOLETIN DE LA SOCIEDAD ESPAÑOLA DE
Cerámica y Vidrio
www.elsevier.es/bsecv

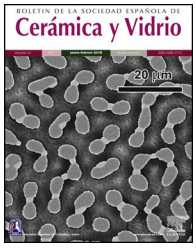

Strontium-Substituted Bioactive Glass-Ceramic Films for Tissue Engineering

Denisa-Alina Draghici[a], *Alina-Andreea Mihai*[a], *Mihail-Octavian Aioanei*[a], *Nadina-Elena Negru*[a], *Adrian-Ionut Nicoara*[a], *Sorin-Ion Jinga*[a], *Dana Miu*[b], *Mihaela Bacalum*[c], *Cristina Busuioc*[a,*]

[a] *University POLITEHNICA of Bucharest, RO-011061 Bucharest, Romania*
[b] *National Institute for Laser, Plasma and Radiation Physics, RO-077125 Magurele, Romania*
[c] *Horia Hulubei National Institute of Physics and Nuclear Engineering, RO-077125 Magurele, Romania*

ARTICLE INFO

Article history:
Received 9 July 2020
Accepted 22 September 2020
Available online 19 October 2020

Keywords:
Glass-ceramics
Coatings
Pulsed laser deposition
Spin coating
Tissue engineering

ABSTRACT

The current study presents a comparison within the framework of 45S5 Bioglass® composition, between two types of coatings, achieved by physical or chemical means. The oxide composition was established within SiO_2–P_2O_5–CaO–MgO–SrO–Na_2O system, while the preparation techniques were pulsed laser deposition and spin coating. The target necessary for laser ablation experiments was achieved via sol-gel route, displaying a quite well-densified microstructure, as well as modified combeite and akermanite as crystalline phases. The resulting layers turned out to be continuous, homogeneous, partially crystalline and nanostructured in texture. The physical approach led to thicker films, which completely veiled the surface irregularities of substrate; moreover, they provided higher apatite-forming ability and better performance in terms of biocompatibility with human fibroblast BJ cells.

Películas vitrocerámicas bioactivas sustituidas con estroncio para la ingeniería de tejidos

Palabras clave:
Vitrocerámica
Recubrimientos
Deposición por láser pulsado
Deposición por centrifugación
Ingeniería de tejidos

RESUMEN

El presente estudio presenta una comparación dentro del marco de la composición 45S5 Bioglass®, entre dos tipos de recubrimientos logrados por medios físicos o químicos. La composición de óxido se estableció dentro del sistema SiO_2–P_2O_5–CaO–MgO–SrO–Na_2O, mientras que las técnicas de preparación fueron deposición por láser pulsado y deposición por centrifugación. El objetivo necesario para los experimentos de ablación láser se logró mediante la ruta sol-gel, mostrando una microestructura bastante bien densificada, así como combeíta modificada y akermanita como fases cristalinas. Las capas resultantes resultaron ser

* *Corresponding author.*
E-mail address: cristina.busuioc@upb.ro (C. Busuioc).
https://doi.org/10.1016/j.bsecv.2020.09.006

continuas, homogéneas, parcialmente cristalinas, nanoestructuradas en textura. El enfoque físico condujo a películas más gruesas, que ocultó completamente las irregularidades superficiales del sustrato; además, proporcionaron una mayor capacidad de formación de apatita y un mejor rendimiento en términos de biocompatibilidad con las células BJ de fibroblastos humanos.

Introduction

Regenerative medicine integrates technologies from engineering and biological sciences to develop new materials that restore, maintain, or enhance tissue morphology or function [1]. In the framework of biocompatibility, the appropriate mechanical properties of designed substitutes are sometimes endangered by phenomena like surface corrosion, interface weakening and body intoxication [2,3]. To avoid this outcome, the applied systems can be optimized [4]; thus, the best way to improve the behaviour of bioinert implants is by coating them with mineral layers, one of the possible choices being glass-ceramic [5]. Bioactive glass-ceramics are formed by controlled crystallization of primary glasses, with the purpose of tailoring the functional properties [6]. Considering tissue engineering field, they can bond to living tissues and improve the growth and proliferation of osteoblasts, stimulation of osteogenesis and angiogenesis, as well as local induction of antibacterial and antifungal effects [7]. In order to trigger favourable biological effects, various metallic cations can be integrated in the parent matrix [8,9]; Sr^{2+} is often employed as glass network modifier, facilitating cells proliferation/differentiation, providing possible antibacterial activity or accelerating bone reconstruction [10–12].

Sol-gel method has a great potential in biomedical engineering, ensuring extended composition ranges and a better control of purity, homogeneity and crystallinity [13,14]. Pulsed laser deposition is a film synthesis technique with the advantages of stoichiometric transfer, absence of contamination and high substrate adhesion, being preferred for growing coatings in hard tissue engineering [15,16]. Additionally, spin-coating is frequently approached for layered biological applications due to its simplicity, thickness control and uniformity ensuring [17,18].

The aim of this work is to synthesize bioactive and biocompatible coatings, starting from the well-known composition of 45S5 Bioglass®, but partially substituting with Sr; it was already demonstrated that low concentration of Sr^{2+} cations enhances proliferations and stimulates osteogenesis [19,20]. In particular, the evaluation of coating method influence is targeted, knowing that pulsed laser deposition is a physical approach, while spin coating is a chemical route. The final samples were analyzed from multiple perspectives to highlight their suitability for tissue engineering applications.

Materials and methods

The target needed for pulsed laser deposition (PLD) experiments was prepared through a wet-chemistry method, adding Sr to the composition of 45S5 Bioglass® [21]: $46.1SiO_2$–$2.6P_2O_5$–16.9CaO–10MgO–5SrO–$19.4Na_2O$ (mol%); the corresponding alkoxides and nitrates/nitrites were processed according to a standard sol-gel procedure, described in a previous paper [22]. Briefly, this type of synthesis involves processes of hydrolysis, condensation and polymerization, by which hydroxy or oxygen bridges are formed, leading in the end to a hydrated oxide network. The dried gel was calcined at 650 °C/2 h, generating a precursor powder, which was further granulated, shaped and sintered at 900 °C/10 h, resulting in a PLD disc. The same precursor solution was employed for spin coating (SC) experiments. The achieved films are listed in Table 1.

The specimens were subjected to a series of characterization methods, as follows: Scanning Electron Microscopy (SEM)

Table 1 – Parameters of coatings deposition.

Sample	Method	Constant parameters	Variable parameters	
PLD-RT	Pulsed laser deposition	-355 nm wavelength -73–74 Mj/pulse energy -30,000 pulses	Substrate temperature	Room temperature
PLD-300		-40 mm distance target-substrate -100 mTorr oxygen pressure -Silicon plate		300 °C
SC-2	Spin coating	-10,000 rpm rotation speed -60 s rotation time -200 °C/5 min drying	Number of layers	2 layers
SC-5		-650 °C/2 h calcining -Titanium plate		5 layers

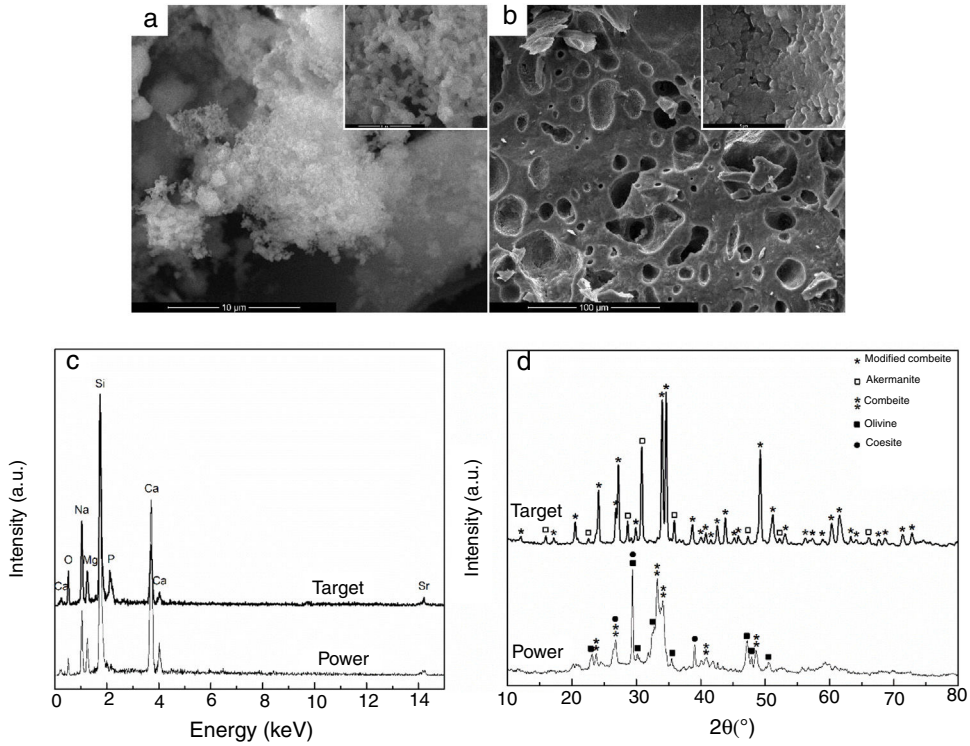

Fig. 1 – (a) SEM images of: (a) powder and (b) target, (c) EDX spectra and (d) XRD patterns of powder and target.

and Energy-Dispersive X-ray Spectroscopy (EDX) with a FEI Quanta Inspect F microscope equipped with EDX probe (30 kV operating voltage, no conductive coating applied), Fourier-Transform Infra-Red Spectroscopy (FTIR) with a Thermo Scientific Nicolet iS50 spectrophotometer (wavenumber ranging between 400 and 2000 cm^{-1}, 4 cm^{-1} resolution), X-ray diffraction (XRD) with a Shimadzu XRD 6000 or PANalytical Empyrean diffractometer (Ni-filtered Cu Kα radiation, 2θ ranging between 10 and 80°, 2°/min scan speed). *In vitro* biological evaluation was performed through Simulated Body Fluid (SBF) immersion for 4 weeks (7.3 *p*H, 37 °C temperature; a surface area of 1 cm^2 was exposed to 2 mL SBF solution, the estimated maximum mass of the coating being of 0.1 mg), as well as MTT assay (absorbance was measured at 570 nm) and fluorescence microscopy (actin filaments were stained with Phalloidin-FITC, nucleus was stained with Hoechst 33342) on human fibroblast BJ cells (ATCC, CRL-2522), as formerly detailed [22].

Results and discussion

The first step was represented by powder and target characterization, the corresponding results being displayed in Fig. 1. Thus, the calcined powder consists of individual nano-sized particles, quasi-spherical or slightly elongated, dispersed or agglomerated (Fig. 1a); the sintering process favoured the appearance of a 3D network crossed by branched porosity (Fig. 1b), but with faceted grains that can reach several microns. EDX investigation confirms the integration of all desired cations within the powder, but some changes in lines relative intensity appear in target spectrum (Fig. 1c), fact that can be correlated with the information provided by XRD patterns. The latter reveal a combination of three crystalline phases in the case of powder: combeite ($Na_4Ca_4Si_6O_{18}$, rhombohedral structure, ICDD-00-075-1686), olivine ($CaSiO_4$, orthorhombic structure, ICDD-00-080-0942) and coesite (SiO_2, monoclinic structure, ICDD-00-083-1833), most likely surrounded by a glassy phase. The target shows a higher crystallinity degree, ensured by two mineralogic phases: a high temperature modification of combeite ($Na_{15.78}Ca_3Si_6O_{12}$, rhombohedral structure, ICDD-00-078-1650) and akermanite ($Ca_2MgSi_2O_7/Sr_2MgSi_2O_7$, tetragonal structure, ICDD-00-083-1815/ICDD-00-075-1736), the rest of elements being incorporated in a vitreous matrix holding the crystals together. Several studies demonstrated promising activity in bone regeneration for both combeite and akermanite [23–27].

The evaluation of the obtained coatings was centralized in Fig. 2. SEM images reveal well-adhered films, with relatively homogeneous microstructure for all samples (Fig. 2a–d). A distribution of droplets specific to PLD method [28] can be identified onto the surface of first two, their size being around hundreds of nm. By increasing substrate temperature, droplets are reduced in number and dimension, while the aspect of exploded entities and tendency of grouping diminish; as well, the grains become better defined and visibly larger. In contrast, the surface of SC layers exhibits a different topography, with roughness that increases as the number of layers gets bigger, which is expectable considering that each additional layer amplifies prior unevenness; process kinetics led to a succession of hills and channels

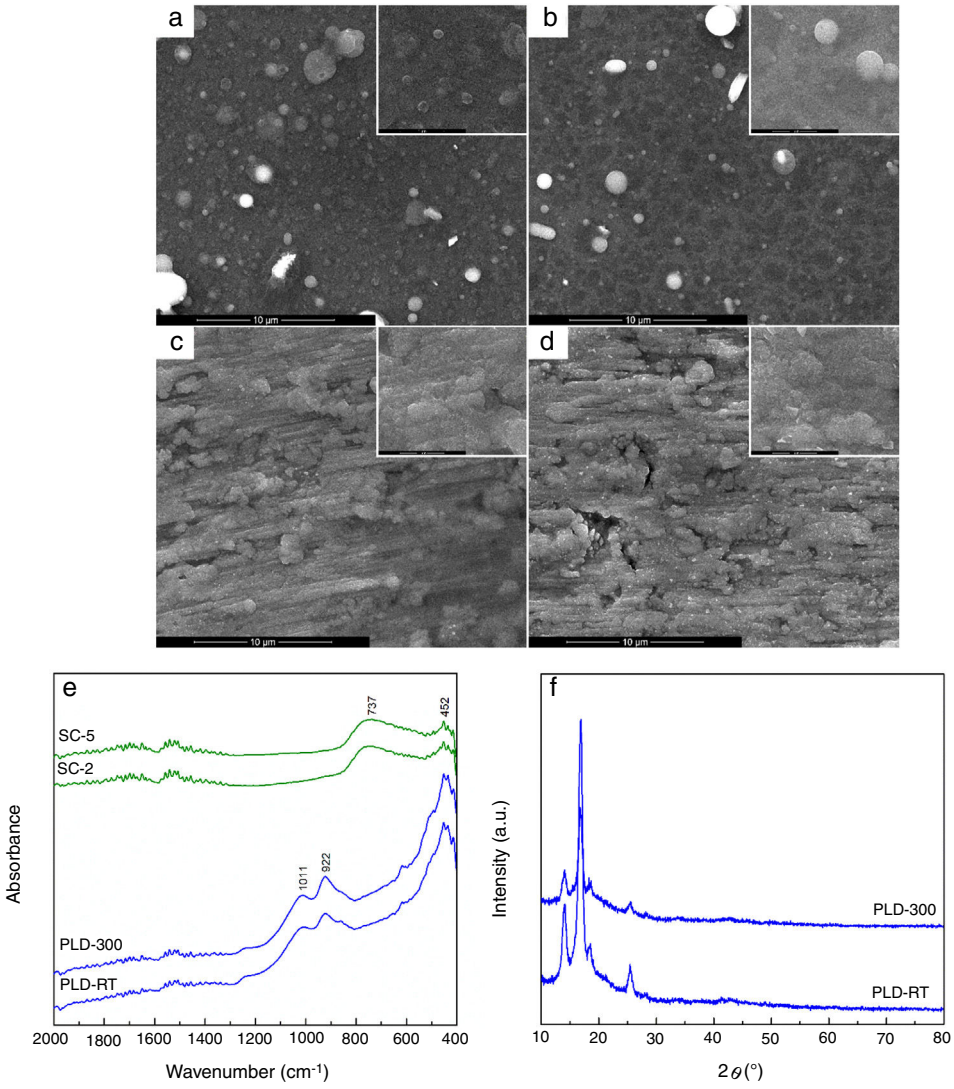

Fig. 2 – SEM images of: (a) PLD-RT, (b) PLD-300, (c) SC-2 and (d) SC-5, (e) FTIR spectra and (f) XRD patterns of films.

distributed in correlation with substrate pattern. At higher magnification, a specific wrinkled texture can be observed, a particularity of SC method [29]. A rough character is favourable for this application because it helps implant osteointegration. Regarding thickness, it was estimated to few hundreds of nm for PLD synthesis and several tens of nm for SC preparation. FTIR spectra validated films growth especially for PLD approach, through the vibrational bands assigned to Si bonding and grouping in the range 800–1100 cm^{-1} (922 cm^{-1} – Si–O bond, 1011 cm^{-1} – Si–O–Si group) and Ca/Mg/Sr–O bonds below 600 cm^{-1} (452 cm^{-1} – Ca–O bond, 493 cm^{-1} – Mg–O bond, 436 cm^{-1} – Sr–O bond) [22]; moreover, due to the low thickness of SC coatings, the predominant band was recorded for passivation oxide layer from substrate surface (737 cm^{-1} – Ti–O bond) (Fig. 2e). The diffractometric assessment evidences a mainly glassy nature of PLD-RT and PLD-300 via the base wide peak associated with short-range order and long-range disorder in the formed network; the narrow peaks representing elevations from the halo one mentioned above could not be clearly attributed to indexed crystalline compounds, but they seem to be proofs of crystalline domains with small size, related either to several types of symmetry in silicon dioxide (SiO_2) ordered species or non-stoichiometric silicates, all embedded within the matrix (Fig. 2f). SC-2 and SC-5, processed identically as the powder used for target preparation, namely the same precursor solution and calcination conditions, can be assimilated with XRD pattern from Fig. 1d; this means a glass-ceramic with combeite, olivine and coesite as crystalline phases. A comparison between the two series of samples, obtained by different methods, highlights the importance of applied temperature: maximum 300 °C for PLD and 650 °C for SC, which is reflected in the crystallinity degree of films.

The changes occurred during SBF immersion were monitored and presented in Fig. 3. All samples were involved in a biomineralization process, proved by the presence of a new surface layer, with different morphological and compositional characteristics. SEM images confirm the deposition of apatite

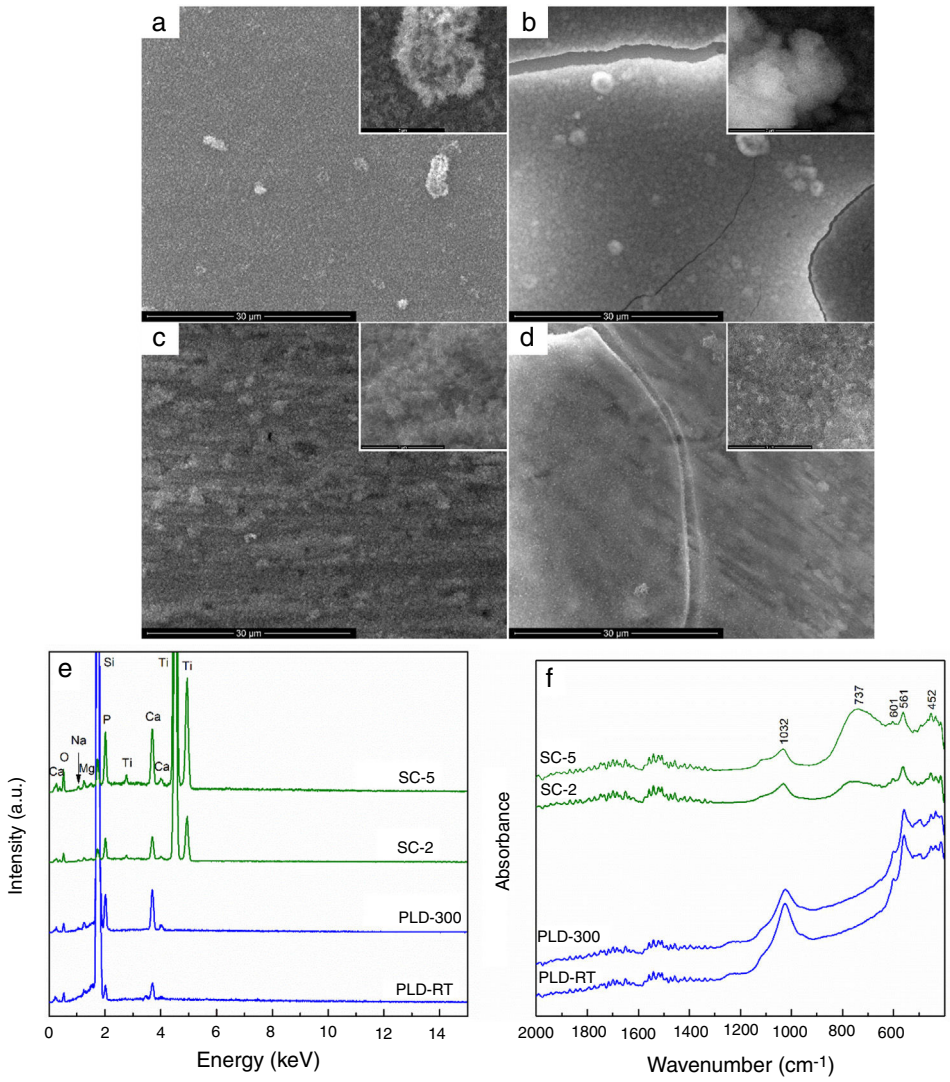

Fig. 3 – SEM images of: (a) PLD-RT, (b) PLD-300, (c) SC-2 and (d) SC-5, (e) EDX spectra and (f) FTIR spectra of films after immersion in SBF.

as a continuous fluffy network of thin and small needles and laminas; the highest yield seems to occur in the case of PLD-300 and SC-5, for which micro-sized cracks can be noticed (Fig. 3a–d). The increase of Ca and P concentrations is clearly suggested in EDX spectra, where the signals for Mg, Sr and Na are shielded (Fig. 3e), while the emergence of phosphate groups specific to apatite is certified by the absorption bands located in FTIR spectra around 1000 and 550 cm^{-1} (Fig. 3f) [22]. Thus, comparing the intensity of these EDX lines with the situation encountered in Fig. 1c, bigger ratios are found between Ca and P on one hand and Mg, Sr and Na on the other after SBF immersion, pointing out that a significant compositional modification took place during 4 weeks of immersion. For PLD coatings, the vibrational characteristics typical of phosphate groups are predominant, evidencing a quantitative superiority of the newly formed shell, in correlation with their higher bioactive potential due to greater thickness; SC films exhibit, besides the signs of phosphate groups, a remaining large band coming from TiO_2 located on substrate surface, indicating reduced thickness for apatite layer. Moreover, a sharp peak is visible at 601 cm^{-1}, well-known as fingerprint of hydroxyapatite. Other researchers also demonstrated that such materials are bioactive, stimulating the process of biological mineralization [30] and sometimes even displaying tailorable biodegradability [31].

Cell viability results shown in Fig. 4 indicate that, compared to Control (cells grown on glass slide in similar conditions), cells growth was not influenced, demonstrating that the investigated surfaces provide a favourable environment for cellular metabolism. The fluorescence images are in accordance with MTT assay, proving that cells morphology, both actin filaments and nucleus, was not affected and their number was not decreased. Thus, the engineered surfaces are cytocompatible and do not hinder cellular proliferation/development, conclusions also formulated by other authors that studied similar systems: such materials support cells adhesion/proliferation

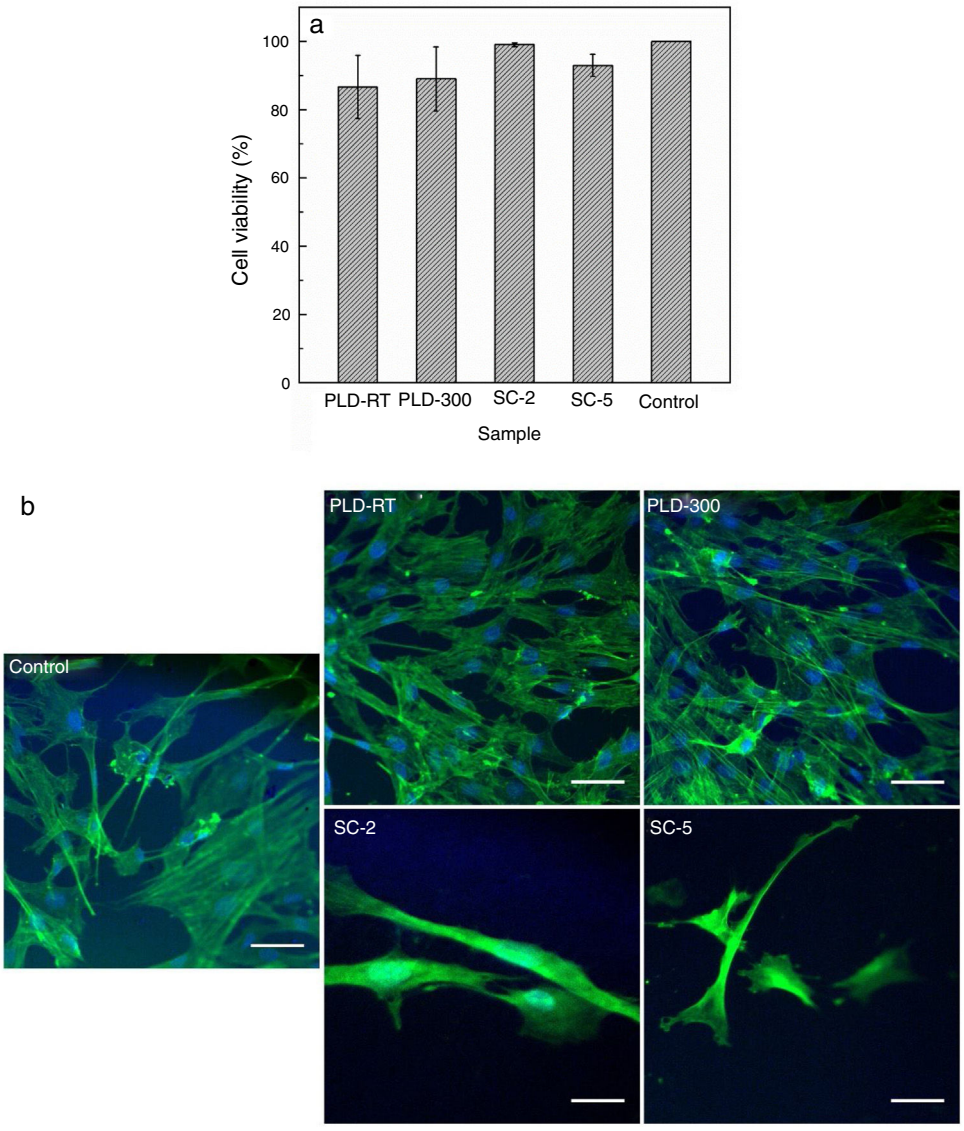

Fig. 4 – (a) Cell viability and (b) fluorescence microscopy images of BJ cells grown on films compared to Control cells grown on glass slide. Scale bar size is 10 μm for all images.

and provide osteogenic potential [24]; in addition to excellent biocompatibility, antibacterial activity could be a supplementary gain [32].

Conclusions

A new bioactive material was developed in the form of coatings, following a composition of 45S5 Bioglass® partially substituted with Sr, namely $46.1SiO_2$–$2.6P_2O_5$–16.9CaO–10MgO–5SrO–$19.4Na_2O$ (mol%) composition. Thin films were grown either by pulsed laser deposition or spin coating, varying either substrate temperature (for pulsed laser deposition) or number of layers (for spin coating), with the purpose of tailoring the properties of future implants. The developed coatings were proven to entirely cover substrate surface, consist of nanometric grains and have a glass-ceramic character. All samples stimulated the process of mineralization and offered positive results in terms of cellular compatibility, but the superior performance of those films achieved by pulsed laser deposition was evident, probably due to their higher thickness, which is equivalent to larger amount of active material; thus, the engineered surfaces are bioactive and promote osseointegration, as well as biocompatible and sustain cell proliferation/development.

REFERENCES

[1] R. Katari, A. Peloso, G. Orlando, Tissue engineering and regenerative medicine: semantic considerations for an evolving paradigm, Front. Bioeng. Biotechnol. 2 (2015) 57.
[2] M. Saini, Y. Singh, P. Arora, V. Arora, K. Jain, Implant biomaterials: a comprehensive review, World J. Clin. Cases 3 (2015) 52–57.

[3] C.L. Romano, H. Tsuchiya, I. Morelli, A.G. Battaglia, L. Drago, Antibacterial coating of implants: are we missing something? Bone Joint Res. 8 (2019) 199–206.
[4] D.T.J. Barone, J.M. Raquez, P. Dubois, Bone-guided regeneration: from inert biomaterials to bioactive polymer (nano)composites, Polym. Adv. Technol. 22 (2011) 463–475.
[5] A. Vladescu, M.A. Surmeneva, C.M. Cotrut, R.A. Surmenev, AntoniacF I.V., Bioceramic coatings for metallic implants, in: I.V. Antoniac (Ed.), Handbook of Bioceramics and Biocomposites, Cham, Springer, 2015, pp. 1–31.
[6] C. Drouet, A. Leriche, S. Hampshire, M. Kashani, A. Stamboulis, M. Iafisco, A. Tampieri, Types of ceramics: material class, in: P. Palmero, F. Cambier, E. De Barra (Eds.), Advances in Ceramic Biomaterials: Materials, Devices and Challenges, Woodhead Publishing Sawston, 2017, pp. 21–82.
[7] S. Omar, F. Repp, P.M. Desimone, R. Weinkamer, W. Wagermaier, S. Cere, J. Ballarre, Sol-gel hybrid coatings with strontium-doped 45S5 glass particles for enhancing the performance of stainless steel implants: electrochemical, bioactive and in vivo response, J. Non-Cryst. Solids 425 (2015) 1–10.
[8] G.S. Lazaro, S.C. Santos, C.X. Resende, E.A. dos Santos, Individual and combined effects of the elements Zn, Mg and Sr on the surface reactivity of a $SiO_2{\cdot}CaO{\cdot}Na_2O{\cdot}P_2O_5$ bioglass system, J. Non-Cryst. Solids 386 (2014) 19–28.
[9] Z. Nescakova, K. Zheng, L. Liverani, Q. Nawaz, D. Galuskova, H. Kankova, M. Michalek, D. Galusek, A.R. Boccaccini, Multifunctional zinc ion doped sol-gel derived mesoporous bioactive glass nanoparticles for biomedical applications, Bioact. Mater. 4 (2019) 312–321.
[10] S. Kargozar, M. Montazerian, E. Fiume, F. Baino, Multiple and promising applications of strontium (Sr)-containing bioactive glasses in bone tissue engineering, Front. Bioeng. Biotechnol. 7 (2019) 161.
[11] M. Ge, K. Ge, F. Gao, W. Yan, H. Liu, L. Xue, Y. Jin, H. Ma, J. Zhang, Biomimetic mineralized strontium-doped hydroxyapatite on porous poly(L-lactic acid) scaffolds for bone defect repair, Int. J. Nanomed. 13 (2018) 1707–1721.
[12] M. Dziadek, B. Zagrajczuk, E. Menaszek, A. Wegrzynowicz, J. Pawlik, K. Cholewa-Kowalska, Gel-derived SiO_2–CaO–P_2O_5 bioactive glasses and glass-ceramics modified by SrO addition, Ceram. Int. 42 (2016) 5842–5857.
[13] S. Taherkhani, F. Moztarzadeh, Influence of strontium on the structure and biological properties of sol-gel-derived mesoporous bioactive glass (MBG) powder, J. Sol-Gel Sci. Technol. 78 (2016) 539–549.
[14] L.A. Quintero Sierra, D.M. Escobar, Characterization and bioactivity behavior of sol-gel derived bioactive vitroceramic from non-conventional precursors, Bol. Soc. Esp. Ceram. Vidr. 58 (2019) 85–92.
[15] R. Negrea, C. Busuioc, I. Constantinoiu, D. Miu, C. Enache, F. Iordache, S.I. Jinga, Akermanite-based coatings grown by pulsed laser deposition for metallic implants employed in orthopaedics, Surf. Coat. Technol. 357 (2019) 1015–1026.
[16] S. Shazia, S. Kedia, A.G. Majumdar, M. Subramanian, S. Sinha, 45S5 bioactive glass coating on Ti6Al4V alloy using pulsed laser deposition technique, Mater. Res. Express 6 (2020) 125428.
[17] C. Busuioc, I. Constantinoiu, M. Enculescu, M. Beregoi, S.I. Jinga, Ceramic thin films deposited by spin coating as coatings for metallic implants, Rev. Rom. Mater. 48 (2018) 401–406.
[18] G. Brunello, H. Elsayed, L. Biasetto, Bioactive glass and silicate-based ceramic coatings on metallic implants: open challenge or outdated topic? Materials 12 (2019) 2929.
[19] C. Bizelli-Silveira, L.A. Abildtrup, R. Spin-Neto, M. Foss, K. Soballe, D.C.E. Kraft, Strontium enhances proliferation and osteogenic behavior of bone marrow stromal cells of mesenchymal and ectomesenchymal origins in vitro, Clin. Exp. Dent. Res. 5 (2019) 541–550.
[20] A. Aimaiti, A. Maimaitiyiming, X. Boyong, K. Aji, C. Li, L. Cui, Low-dose strontium stimulates osteogenesis but high-dose doses cause apoptosis in human adipose-derived stem cells via regulation of the ERK1/2 signaling pathway, Stem Cell Res. Ther. 8 (2017) 282.
[21] I. Ochoa, J.A. Sanz-Herrera, J.M. Garcia-Aznar, M. Doblare, D.M. Yunos, A.R. Boccaccini, Permeability evaluation of 45S5 Bioglass®-based scaffolds for bone tissue engineering, J. Biomech. 42 (2009) 257–260.
[22] R.I. Schitea, A. Nitu, A.A. Ciobota, A.L. Munteanu, I.M. David, D. Miu, M. Raileanu, M. Bacalum, C. Busuioc, Pulsed laser deposition derived bioactive glass-ceramic coatings for enhancing the biocompatibility of scaffolding materials, Materials 13 (2020) 2615.
[23] E. Fiume, G. Serino, C. Bignardi, E. Verne, F. Baino, Bread-derived bioactive porous scaffolds: an innovative and sustainable approach to bone tissue engineering, Molecules 24 (2019) 2954.
[24] A. Thomas, J. Bera, Preparation and characterization of gelatin-bioactive glass ceramic scaffolds for bone tissue engineering, J. Biomater. Sci. Polym. Ed. 30 (2019) 561–579.
[25] L.A. Adams, E.R. Essien, Bioactivity of quaternary glass prepared from bentonite clay, J. Adv. Ceram. 5 (2016) 47–53.
[26] H. Mohammadi, Y.M.B. Ismail, K.A. Shariff, A.F.M. Noor, Effect of substitutional strontium on mechanical properties of akermanite ceramic prepared by solid-state sintering, Mater. Today Proc. 17 (2019) 929–936.
[27] V.B. Bhatkar, N.V. Bhatkar, Combustion synthesis and photoluminescence study of silicate biomaterials, Bull. Mater. Sci. 34 (2011) 1281–1284.
[28] C. Busuioc, G. Voicu, I.D. Zuzu, D. Miu, C. Sima, F. Iordache, S.I. Jinga, Vitroceramic coatings deposited by laser ablation on Ti-Zr substrates for implantable medical applications with improved biocompatibility, Ceram. Int. 43 (2017) 498–5504.
[29] G. Voicu, D. Miu, C.D. Ghitulica, S.I. Jinga, A.I. Nicoara, C. Busuioc, A.M. Holban, Co doped ZnO thin films deposited by spin coating as antibacterial coating for metallic implants, Ceram. Int. 46 (2020) 3904–3911.
[30] R. Du, J. Chang, Preparation and characterization of bioactive sol-gel-derived $Na_2Ca_2Si_3O_9$, J. Mater. Sci. Mater. Med. 15 (2004) 1285–1289.
[31] Q.Z. Chen, I.D. Thompson, A.R. Boccaccini, 45S5 Bioglass®-derived glass-ceramic scaffolds for bone tissue engineering, Biomaterials 27 (2006) 2414–2425.
[32] B. Cabal, L. Alou, F. Cafini, R. Couceiro, D. Sevillano, L. Esteban-Tejeda, F. Guitian, R. Torrecillas, J.S. Moya, A new biocompatible and antibacterial phosphate free glass-ceramic for medical applications, Sci. Rep. 4 (2014) 5440.